POLITECNICO
MILANO 1863

SCUOLA DI INGEGNERIA INDUSTRIALE
E DELL'INFORMAZIONE

Executive Summary of the Thesis

Engineering of Rashba spin textures in chalcogenide alloys

Laurea Magistrale in Engineering Physics- Ingegneria Fisica

Author: Federico Belponer

Advisor: Prof. Matteo Cantoni

Co-advisor: Prof. Christian Rinaldi, Dr. Luca Nessi

Academic year: 2020-2021

1. Introduction

Spintronics deals with injection, control, and detection of spin currents in order to integrate the spin degree of freedom into semiconductor-based conventional electronics. The emerging branch of *spin-orbitronics* aims to reach this goal by exploiting non-magnetic materials that present a large Spin-Orbit Coupling (SOC). This characteristic allows to bridge the two electronic variables (charge and spin) via spin-to-charge conversion (SCC) processes. High SOC was found, e.g., in heavy metals, Rashba interfaces and topological insulators.

The recently discovered FErroelectric Rashba Semiconductors (FERSC) class of materials, whose father compound is GeTe, showed intriguing spin properties which can be tuned by means of the non-volatile ferroelectric polarisation [2]. This effect was proved to resist even at room temperature (RT) in GeTe [5], thus making this material a valid candidate for tunable spintronic devices.

In general, chalcogenides are good candidate members of the FERSC class and among them there is SnTe, already known for being a Topological Crystalline Insulators (TCI) [4]. SnTe presents a stable cubic structure at RT and a ferroelectric one (α-phase) at low temperature ($T < 100\ K$). In its distorted structure, SnTe was predicted to belong also the FERSC class, while preserving its topological nature [3].

In the following, we present the investigations conducted on the ternary alloy $Ge_xSn_{1-x}Te$ (GST): we tried to engineer the electronic properties of the SnTe by doping it with Ge atoms, aiming at a a FERSC material with coexisting topological and Rashba features. The studies were conducted from a material science point of view: growing the samples by Molecular Beam Epitaxy (MBE) and characterizing them with *in-situ* spectroscopy and diffraction and by mean of spin- and angle-resolved photoemission spectroscopy (S-ARPES), performed at the APE beam-line of Elettra synchrotron in Trieste.

The characterization of SCC performances usually requires the use of ferromagnetic heterostructures for spin-injection. An alternative to this would be *in-vacuum* direct spin-injection with a spin-polarized electron beam. The PoliFab laboratory presents the instrumental setup for such scope [1], but improvements were needed to reduce the spot size (in order to target patterned structures) and increase the stability of the electron beam. In this thesis, an improved version of the electron gun control system is reported.

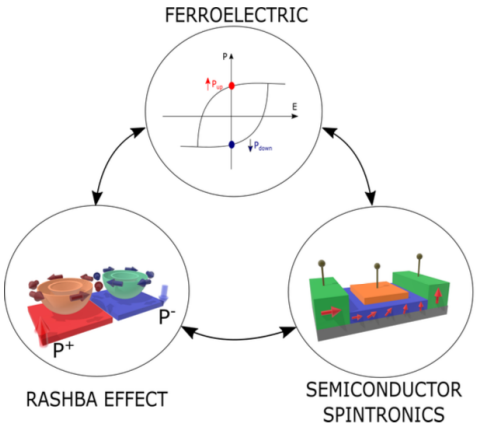

Figure 1: Schematic representation of the physical properties of ferroelectric Rashba semiconductors (FERSC).

2. Theoretical overview

Rashba effect is a relativistic effect caused by the spin-orbit coupling (SOC) in non-centrosymmetric systems that leads to a momentum dependent energy shift for the two states of spin polarization. For a two-dimensional electron gas, the energy dispersion is the following, also reported in fig. 2a:

$$E_{\pm} = \frac{\hbar^2 k^2}{2m} \pm \alpha_R |k| \qquad (1)$$

where the intensity of Rashba splitting is quantified by the Rashba parameter α_R or, alternatively, by the Rashba momentum k_R defined as the momentum at which the peak of Rashba bands (RB) is located.

RB present locking between momentum and spin of electrons, which leads to SCC processes such as Spin Hall Effect (SHE) and Rashba-Edelstein Effect (REE)[1], that are employed for spin-orbitronic devices.

GeTe is a prototypical crystalline ferroelectric, with a stable polarization along the (111) direction of $\sim 60\mu C \cdot \mathrm{cm}^{-2}$, and presents a giant Rashba splitting at the Z point of the Brillouin zone (fig. 2b), with $\alpha_R \sim 5$ Å (larger than most of other materials, such as BiTeI, with $\alpha_R = 3.8$ Å).

On the other side, SnTe shows a cubic phase at RT which, thanks to crystalline symmetries, originates topologically protected surface states. Due to topological robustness, the distortion along the (111) direction for the α-SnTe preserves two Dirac cones along the $\bar{\Gamma}\bar{Z}$ direction

[1]The Inverse of these processes is also possible, corresponding to ISHE and IREE.

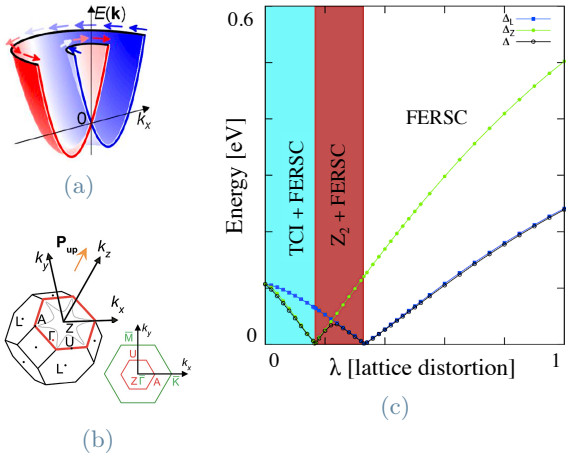

Figure 2: (a) Example of Rashba bands for a 2-DEG with the arrows representing the spin polarization direction. (b) First brillouin zone of bulk SnTe with the projections for the [111] direction. (c) Topological phase diagram for SnTe, showing the distribution of the energy gaps around Z (ΔZ), L (ΔL) and the minimum value Δ as a function of the lattice distortion λ from cubic ($\lambda = 0$) to rhombohedral ($\lambda = 1$) structure. Adapted from [3].

of reciprocal space (fig. 2b).

Theoretical predictions [3] have shown how the distortion of the cubic structure can effectively modify the electronic band dispersion of SnTe leading to the cohexistance of different states: from $\mathbb{Z}_2$-TI+FERSC, to TCI+FERSC, to pure FERSC at full rhombohedral distortion, as shown in fig. 2c. The opportunity to tune the properties of SnTe induced us to search for engineering solutions to this scope, such as the doping of SnTe with Ge in order to obtain a FERSC material that would present intermediate properties between the two (topological surface states and bulk RB), thus proving the possbility to tune SCC properties of this alloy.

3. Chalcogenide alloy samples $Ge_xSn_{1-x}Te$

In order to investigate the band structure of the ternary alloy $Ge_xSn_{1-x}Te$ (GST) at different Ge doping concentrations x, we considered a set of four samples, presented in table 1.

3.1. Samples growth and in-situ characterization

The samples growth started from $5 \times 10\mathrm{mm}^2$ previously grown heterostructures of

	x [%]	SnTe t[nm]
ST1	31.3 ± 4.6	20 ± 1
ST2	43.0 ± 3.0	10 ± 1
ST3	54.2 ± 1.4	5 ± 1
GT	100	0

Table 1: Samples list, presenting the Ge concentration x ($Ge_xSn_{1-x}Te$) and the deposited thickness of SnTe t.

GeTe(111)/Sb/Si(111)($\sqrt{3} \times \sqrt{3}$). The use of GeTe as underlayer for epitaxial growth of SnTe aims to stabilize its ferroelectric phase by dipolar interaction. SnTe was grown on the GeTe film (18 nm thick) by mean of molecular beam epitaxy (MBE) from a single crucible containing SnTe fragments in the amorphous/ multicrystalline phase (deposition temperature 570 K and rate of ~ 2Å/min).
The doping procedure consisted in an annealing-driven interdiffusion of Ge atoms in the SnTe matrix (heating at T=620 K for 30'): the doping can be controlled by a careful tuning of the SnTe layer thickness (from 5 to 20 nm) in order to set the Ge concentration x in uppermost layers (to which the used spectroscopic techniques are sensitive).
The crystallinity of samples was verified by Low Energy Electron Diffraction (LEED) and X-ray Photoemission Diffraction (XPD), reported in fig. 3a, while the stoichiometry was performed with X-ray Photoemission Spectroscopy (XPS), reported in fig. 3b. The obtained samples show a variable concentration, computed by XPS stoichiometry, of Ge with the thickness, as shown in table 1, and high crystalline quality before and after the doping process, as proved by XPD.

3.2. ARPES and S-ARPES measurements

The spectroscopic analysis performed at the Elettra synchtron consisted in ARPES and S-ARPES measurements. The samples were first processed to remove the protective layer (Te, 20 nm) that was deposited after growth to prevent surface contamination during exposure to ambient pressure.
Analysing the samples at different photon energies (from 16 eV to 25 eV), it is possible to

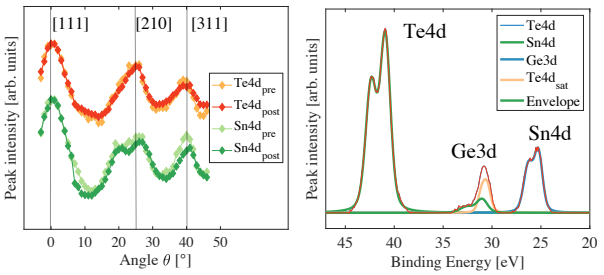

(a) (b)

Figure 3: (a) XPD spetra for Sn and Te before and after the in-situ annealing for doping. (b) XPS spectrum of ST1 performed at grazing angle (60°) used for in situ stoichiometry, showing different element components and a satellite peak originating from the Te4d peak

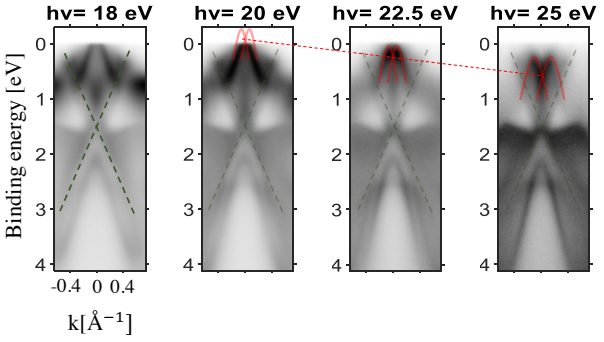

(a) (b) (c) (d)

Figure 4: Photon energy dependent ARPES measurements for sample ST1, along the ZA direction at 77 K. (a-f) Carpets for $h\nu$ from 18 eV to 25 eV. Bulk Rashba bands are highlited in red, while the shift of their intersection with the varying photon energy with the dashed red line. Green dashed lines highlight the conic surface states.

distinguish bulk and surface states, as reported in fig. 4 for sample ST1. The green dashed line highlights the surface states, with the same shape of the SnTe topological Dirac cone. The Rashba bulk bands (RB) are highlighted in red. The presence of RB constitutes a proof of the distorted structure of GST, since they originate from the inversion symmetry breaking.

ARPES measurements were performed at different temperatures: T=77 K, 150 K, and T=320 K. The observed stability of band structure with temperature allowed to demonstrate the structural stability of the alloy up to RT, a fundamental achievement for applications.
The comparison of ARPES measurements on different samples (varying x, at fixed photon energy $h\nu = 20$ eV) is reported in fig. 5a-d and allows to retrieve two main trends for the elec-

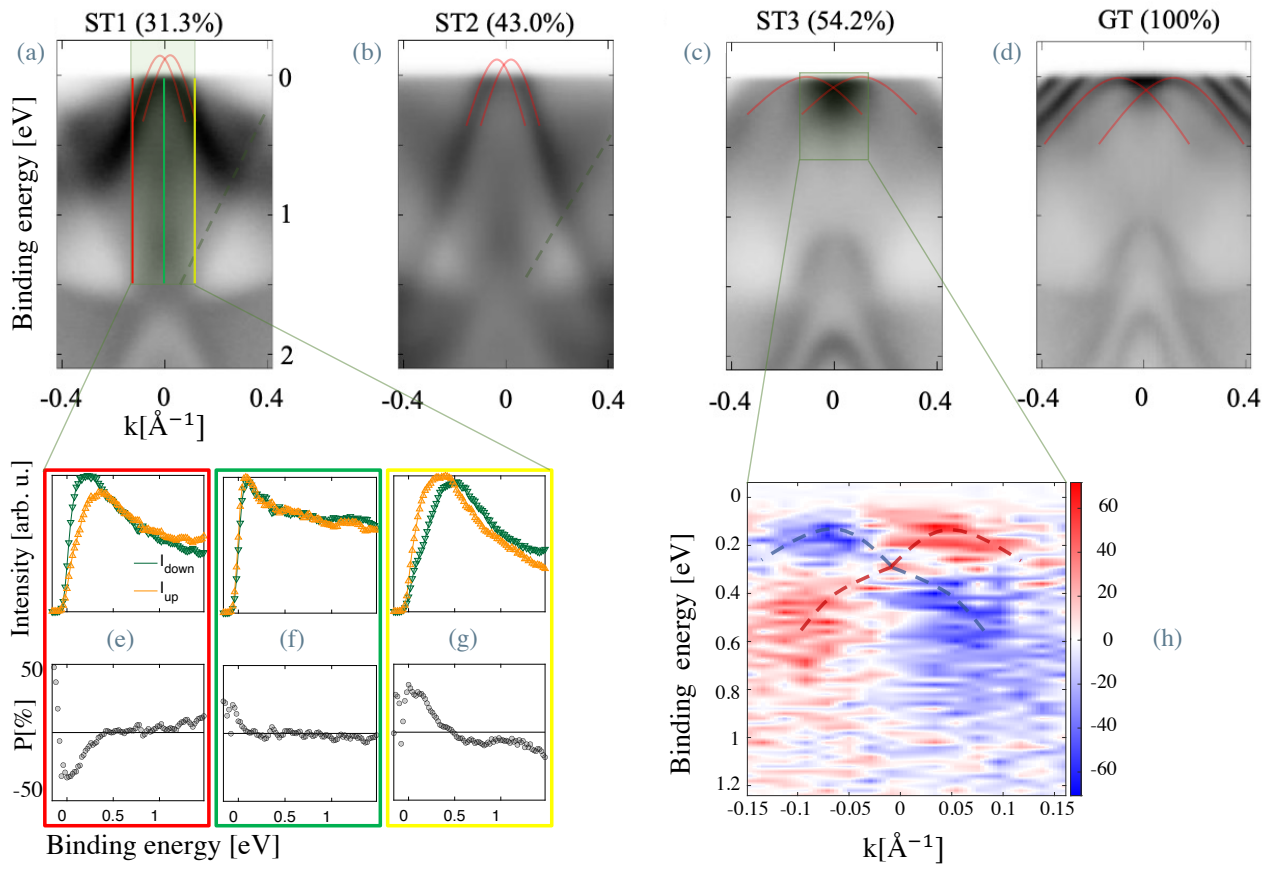

Figure 5: Panels (a), (b), (c), (d) show the ARPES carpets, performed along the ZA direction at $h\nu = 20$ eV and T= 77 K, of the four samples with different Ge concentrations (written in brackets). The bulk Rashba bands are highlighted in red, while the conic surface states are highlighted with a dashed green line, where the states are visible. In panels (e), (f), (g) are reported the spin dependent spectra, at fixed momentum k_x and k_y, for sample ST1. The intensities for the two opposite polarization states are respectively represented in yellow and green, while the calculated polarization is reported below. In (h) is reported the spin-sensitive ARPES for sample ST3, showing the distribution of the two spin-polarized Rashba bands (polarization percentage is expressed by color intensity).

tronic band structure with the increase in Ge concentration:

- increase in the splitting of Rashba bands (highlighted by the red parabola-shaped lines);
- vanishing of the conic surface states (highlighted, where visible, by a green dashed line).

The overall comparison shows the possibility to tune the contribution of these two types of bands by changing the doping.

RB, highlighted in red, were proved to be oppositely spin-polarized by mean of spin-resolved measurements. Spin scans at fixed momentum k_x and k_y are presented in fig. 5e-g for sample ST1. It can be noted that acquisitions at two opposite points along the ZA direction ($+k$, $-k$) show opposite distribution of spin-polarized bands, while the central panel ($k = 0$) shows no polarization, as expected from Rashba splitting theory.

For sample ST3, an example of two-dimensional spin-resolved carpet along the ZA direction is reported in fig. 5h, showing the opposite polarization of the two Rashba bands.

3.3. Discussion

The results shown in previous sections have been compared to Density Functional Theory (DFT) calculations, performed by collaborators at CNR-SPIN, L'Aquila. Considering the Rashba momentum (see section 2) as the estimate for the amount of Rashba splitting, it is possible to show its increasing trend with Ge doping. The experimental data of k_R-vs-%Ge,

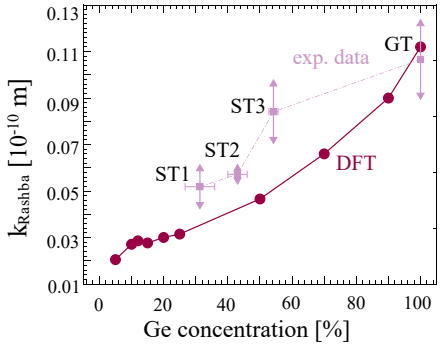

Figure 6: Experimental data for the Rashba k vector along ZA (i.e. the modulus of k-vector at which the valence band has its maximum) compared to the ones predicted by DFT.

compared with the DFT calculations, are reported in fig. 6.
The results are so far in agreement with the qualitative trend of the prediction, but further studies are needed for a broader and quantitative interpretation.

4. Electron gun: design and realization of the control unit

The electron gun system present at PoliFab consists of: (i) a NEA-prepared GaAs photocathode (E_{gap}=1.42 eV), (ii) an IR laser to induce photemission from GaAs (λ = 808 nm) and (iii) the electron gun, which is made by a set of electrostatic lenses for electron beam propagation and focusing [1]. A set of highly stable potentials is needed in this last for transmission stability and spot size control. These potentials are controlled by a control unit.
The previously present Control Unit (CU) was made of seven industrial power supplies, analogically controlled with potentiometers. The main limitation of this system were the output voltage range (0-430 V), not allowing to reach the optimal focus configuration, and the impossibility to automatically acquire the currents flowing into the electrodes (the misalignment of the electron beam leads to absorption of it at the electrodes, resulting in a detectable current to be minimized to improve the gun transmission).
Part of the thesis activity consisted in the design and realization of a new CU with better performances. This apparatus is digitally controlled via computer (easiness of use and reproducibility

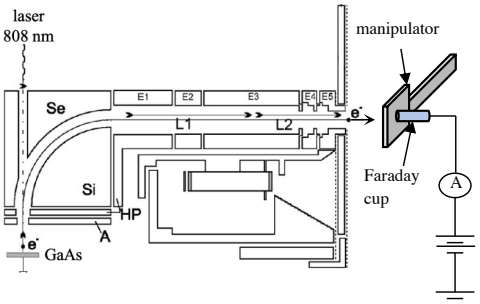

(a)

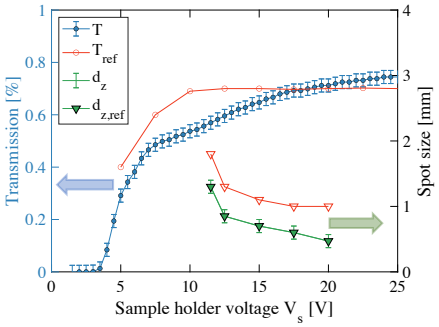

(b)

Figure 7: (a) Setup for the electron beam characterization. The Faraday cup with entrance diameter 0.5 mm is located in front of the output. By moving the manipulator, it is possible to characterize the spatial distribution of the beam. The results are reported in (b), reporting the total transmission and the spot size of the beam at the varying sample manipulator potential (configuration with grounded photocathode). The experimental data are compared with the reference value for the previous setup.

of experiments) and uses 2 high-voltage power supplies as maximum voltage reference (500 V and 700 V) that are then split onto seven independently controlled channels, that power the seven electrodes of the gun. A floating ammeter module is also added to every electrode to acquire and visualize via software all the electrodes currents in parallel. The overall performance of the CU was first tested on bench and then on the electron gun setup with an experiment to determine the gun transmission (ratio between the total output current and the one emitted by photocathode) and beam size. The output voltages were found to be stable after a thermal drift during warm up and no relevant cross-talking problems emerged.
Transmission experiments were performed varying the kinetic energy of the electrons reaching the sample and acquiring the signal with a Faraday cup (entrance diameter 0.5 mm) mounted on

the high-precision xyz-manipulator, as shown in fig. 7a. By moving the manipulator along two orthogonal axes, it is possible to evaluate the shape of the beam.
The results for the total transmission and the beam spot size (calculated as the diameter at FWHM) are reported in fig. 7b. The data are compared with the ones of the previous CU, taken as a reference. An improvement of $\sim 50\%$ (from 1 mm to 0.5 mm) in the beam spot size was obtained, while the overall transmission performances were almost preserved. Further testing is still needed to improve these performances, but preliminary results already show an improvement on the quantities of interest, being the spot size and the functionality of the control unit.

5. Conclusions

To summarize, we showed the possibility to stabilize the ferroelectric phase of SnTe up to room temperature by mean of Ge doping, which constitutes an extremely important achievement for possible applications. The ARPES analysis of the GST alloy has demonstrated the possibility of engineering its band structure, e.g. the Rashba band splitting, with the amount of Ge doping: larger splitting is obtained for increasing Ge concentration. Furthermore, the experimental results were supported by independent DFT calculations, which report an analogous trend for the effect.
For what concerns the instrumental improvements on the electron gun setup, the realization of an easy-to-use software controlled control unit allowed to obtain a beam with a smaller spot size of 0.5 mm ($\sim 50\%$ of the previous). This result is mainly related to the increased voltage range available (0-700 V). The solution developed, requiring only two high-voltage power supplies (HVPS), also constitutes an extremely economic alternative to the use of seven independent industrial HVPS.

6. Acknowledgements

The author thanks the Physics department of Politecnico di Milano for the laboratories instrumentation provided. Special thanks to prof. Cantoni, prof. Rinaldi and prof. Bertacco for supervising the thesis. Thanks to Luca and Federico for having shared the experimental work experience and having thought me many things along the way. Last but not least, I want to thank my family, friends and Martina, for the constant support during these years.

References

[1] Cantoni, M. and Bertacco, R. (2004). High efficiency apparatus for spin polarized inverse photoemission. *Review of scientific instruments*, 75(7):2387–2392.

[2] Picozzi, S. (2014). Ferroelectric rashba semiconductors as a novel class of multifunctional materials. *Frontiers in Physics*, 2:10.

[3] Plekhanov, E., Barone, P., Di Sante, D., and Picozzi, S. (2014). Engineering relativistic effects in ferroelectric snte. *Physical Review B*, 90(16):161108.

[4] Tanaka, Y., Ren, Z., Sato, T., Nakayama, K., Souma, S., Takahashi, T., Segawa, K., and Ando, Y. (2012). Experimental realization of a topological crystalline insulator in snte. *Nature Physics*, 8(11):800–803.

[5] Varotto, S., Nessi, L., Cecchi, S., Sławińska, J., Noël, P., Petrò, S., Fagiani, F., Novati, A., Cantoni, M., Petti, D., et al. (2021). Room-temperature ferroelectric switching of spin-to-charge conversion in germanium telluride. *Nature Electronics*, 4(10):740–747.